Australian Government
Department of Defence
Defence Science and
Technology Organisation

Footprint Reduction for the Acoustic Electric Feedthrough Technique

Scott Moss, Jeremy Skippen, Michael Konak and Ian Powlesland

Air Vehicles Division
Defence Science and Technology Organisation

DSTO-TR-2395

ABSTRACT

This report outlines progress towards reducing the footprint of the DSTO Acoustic Electric Feedthrough (AEF). The AEF approach is being explored as a potential means of wirelessly powering in situ structural health monitoring systems embedded within aircraft and other high value assets. In previous work it was shown that power and data communications can be transmitted ultrasonically through thin aluminium plate using an AEF formed with 38 mm diameter piezoelectric disks. In this report it is shown that a small-sized AEF system formed using 10 mm diameter piezoelectric disks (equating to a footprint reduction of 93%) has a power transfer efficiency of 42% and data transfer rate of 115 kBits per second, equivalent to the capabilities of the previously examined AEF arrangments with significantly larger footprint. Two-dimensional finite-element models are developed and shown to have sufficient fidelity to assist with future AEF design and optimisation.

Published by

Air Vehicles Division
DSTO Defence Science and Technology Organisation
506 Lorimer St
Fishermans Bend, Victoria 3207 Australia

Telephone: (03) 9626 7000
Fax: (03) 9626 7999

AR-014-730
March 2010

APPROVED FOR PUBLIC RELEASE

Footprint Reduction for the Acoustic Electric Feedthrough Technique

Executive Summary

This report has examined the modelling, characterisation and manufacture of an *Acoustic Electric Feedthrough (AEF)* arrangement with a significant footprint reduction compared with AEF geometries previously examined by DSTO. The ultimate aim of the work is to develop a small, robust, detachable AEF system capable of passing power and communications through the aluminium skin of an aircraft using ultrasound. This has the potential to foster autonomous operation of integrated structural health monitoring systems currently being developed for potential application to RAAF aircraft. An AEF arrangement operates via two piezoelectric elements, located collinearly on opposite sides of a metal plate used to simulate an aircraft metallic skin. A piezoelectric element is excited at its thickness mode anti-resonance frequency producing ultrasound that passes through the metal plate and is received by a second element located on the opposite side of the plate. Earlier AEF arrangements investigated by DSTO had a 38 mm diameter. The AEF arrangement examined in this report has a diameter of 10 mm, equating to footprint reduction of 93%. This report demonstrates that a *10 mm AEF arrangement:* (i) has the same power transfer efficiency, (ii) is capable of transferring the same amounts of power, and (iii) has the same data transfer rate as the much larger variant. This report also demonstrates that a *10 mm AEF arrangement* is capable of charging an 80 mA.hr Li-ion battery. The one-dimensional AEF model previously developed by DSTO was unable to accurately model the *10 mm AEF arrangement* due to the aspect ratio of the piezoelectric elements employed. Two-dimensional finite-element models are developed and shown to have sufficient fidelity to assist with future AEF design and optimisation.

Authors

Scott Moss
Air Vehicles Division

Scott Moss received a B.App.Sci. in Applied Physics in 1990 from the Royal Melbourne Institute of Technology, winning the Walter Boas Memorial Prize that year. He was a contract lecturer/tutor at RMIT during 1991-1992, studied towards a PhD at RMIT during 1993-1996 investigating electrical contacts to high temperature superconductors, was a Research Associate at the University of Wollongong in 1997 investigating Uranium doping of Bismuth HTS tapes, and a Junior Lecturer at the University of Tasmania in 1998-1999 teaching physics and electronics. He conferred his PhD in 1999, the same year he joined DSTO Air Vehicles Division to mainly work on the development of the 'smart patch' composite repair for the RAAF F/A-18. In 2003 he was awarded a Defence Science Fellowship and spent a year at UCLA investigating energy harvesting from aircraft structures. This work continues as an exploration of techniques for powering, and communicating with, structural health monitoring devices.

Jeremy Skippen
Air Vehicles Division

Jeremy Skippen is currently three years into completing the double degree of Bachelor of Engineering (Robotics and Mechatronics) and Bachelor of Science (Computer Science). He is on a one-year contract with DSTO Smart Structures and Advanced Diagnostic Group as an Industrial Based Learning student, where he is developing an Acoustic-Electric connector that provides half-duplex communications and downstream power.

Michael Konak
Air Vehicles Division

Michael Konak has a Certificate of Technology in Electronics from the Royal Melbourne Institute of Technology (RMIT) 1980, a B.Eng.(Hons.) in Electronic Engineering also from RMIT in 1989, and a Masters Degree in Engineering from University of Adelaide. He joined Structures Division at the Aeronautical Research Laboratory Melbourne in 1988. He has been involved in the design and implementation of instrumentation systems used for fatigue analysis of aircraft structures and contributed to research on a self-powered health monitoring system and vibration supression using piezoelectric devices, related to aircraft structures. He is currently a Science and Technology Officer in the Air Vehicles Division at DSTO Melbourne.

Ian Powlesland
Air Vehicles Division

Ian Powlesland joined the then Aeronautical Research Laboratories in 1972 and has predominantly worked with structural testing instrumentation since that time. This has included early dedicated portable signal averaging equipment, Nomad, CT4 and F/A-18 fatigue test control systems and some field trials. Currently he is working in the field of autonomous damage and loading sensors for managing an aging fleet.

Contents

Figures

1. Introduction

The Australian Defence Science and Technology Organisation (DSTO) is developing various in situ structural health monitoring (SHM) systems [1, 2, 3, 4, 5] for potential use in high value platforms across the Australian Defence Force. In 2008 the DSTO Compact Multi Parameter Load Evaluation unit (CMPLE) [6] was flight trialled on a Royal Australian Air Force (RAAF) DHC-4 Caribou aircraft. The CMPLE is a rapidly installed and detachable flight loads and acceleration measurement system. The flight trial plan involved mounting CMPLE units at various external locations on an aircraft. The units recorded flight data during three flight trials. Each unit was installed in less than one hour before the flight trial and then removed after the trial was completed. Total flight time for the units was just over four and a half hours. The initial flight trials of this low-cost technology have been used to show that the CMPLE system can assist the airworthiness authority in assessing the structural integrity of the aging RAAF fleet. The CMPLE system could be employed to: (i) continuously monitor airframe loads and accelerations during flight, (ii) detect damage and damage growth and other structural problems, and (iii) provide a basis for near-real-time damage assessment. This technology could also potentially permit a safe reduction in inspection and regular maintenance costs and therefore substantially affect aircraft through-life support costs.

To increase the usefulness of the CMPLE system, an Acoustic Electric Feedthrough (AEF) [7, 8, 9] system is being investigated by the DSTO as a means of providing power and two-way communications to a CMPLE unit that has been mounted at a location within an aircraft where physical access is difficult. An AEF arrangement operates via two axially aligned piezoelectric elements, mounted on opposite sides of a metal plate. The AEF concept was initially proposed by Hu *et al* [10] who modelled an AEF from first principles, and was extended by Sherrit *et al* [11]. The AEF model implemented by Hu *et al* and Sherrit *et al* consisted of a metal plate sandwiched between two piezoelectric layers. Previous work by the DSTO has examined the behaviour of an AEF arrangement formed using piezo-ceramic disks with diameter 38 mm and thickness 2 mm, across an aluminium plate with thickness 1.6 to 5 mm. In the previous DSTO work [7-9] one-dimensional modelling of the various AEF arrangements was carried out using LTspice [12], and found to be reasonably accurate.

One of the concerns with the AEF arrangements explored by the DSTO to date has been the inconveniently large area required by the 38 mm diameter piezo-ceramic disks. In an attempt to resolve this matter, the DSTO has examined an AEF system formed using disks with 10 mm diameter and 2 mm thickness, which has resulted in a substantial footprint reduction for the AEF arrangement. A side effect of moving to smaller diameter piezo-ceramic disks is that the one-dimensional LTspice AEF models utilised in earlier reports become unreliable as the disk geometry moves from plate-like towards cylindrical, that is once the diameter to thickness ratio falls below 10. It was expected that a two-dimensional modelling tool would be required to explore the new small-footprint AEF arrangements. For this purpose two software packages capable of modelling piezoelectric systems were chosen, the ATILA-Light Finite Element Modelling (FEM) software [13] and the COMSOL Multiphysics Solver [14].

This report will discuss the characterisation of an AEF arrangement formed using piezo-ceramic disks with diameter 10 mm and thickness 2 mm, with comparison against modelled results produced using piezoelectric modelling software, and also against previously reported results from AEF arrangements with 38 mm diameter disks.

2. Experimental

This section examines the manufacture of the AEF arrangement and the associated laboratory measurements and modelling required to characterise the system. An AEF arrangement was formed using two Lead-Zirconium-Titanate elements (chemical formula $PbZr_xTi_{1-x}$, with acronym PZT). The elements had a disk geometry with diameter 10 mm and thickness 2 mm, and were bonded across the centre of a square aluminium plate with 600 mm side length and 1.6 mm thickness. Figure 1 shows a schematic of the physical interface of the AEF arrangement. With reference to Figure 1, the AEF technique can be summarised thus: a sinusoidal voltage with an approximate frequency of 1 MHz is applied to the transmit PZT element where it is transduced into a mechanical wave, which then passes across the physical interface as ultrasound, arriving at the receive PZT element where the wave energy is transduced back into an electrical form.

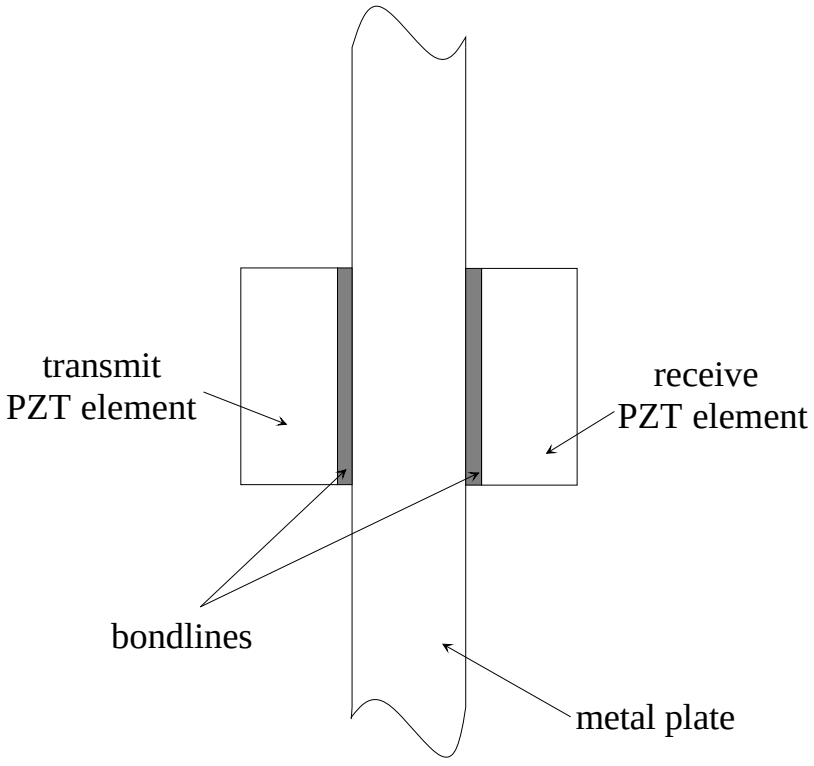

Figure 1: Schematic showing the Physical Interface of an Acoustic Electric Feedthrough (AEF)

A number of factors need to be considered when experimentally investigating an AEF arrangement. These factors are listed here and discussed in detail in references [7 - 9]:

(i) *PZT elements.* The hard PZT ceramic Pz26 [15] was used for all investigations described in this report, with all elements having 2 mm nominal thickness. Matched pairs of Pz26 transmit and receive elements were selected for use in the AEF experiments, with pairs having matching thickness resonant frequencies near 1 MHz. See references [7-9] for further discussion of element matching.

(ii) *Supply impedance*. All measurements were performed using an AG1021 100 W RF power amplifier (nominal 50 Ω output impedance) to drive the transmit PZT element.

(iii*) Constant power (or voltage) source*. During frequency sweeps (as described in section 2.1.1), the output of the power amplifier was computer-controlled to ensure that the apparent input power (or voltage) remained constant.

(iv) *Load resistance.* An optimised resistive load was used for the power transfer experiments discussed in section 2.1.1.

(v) *Diodes*. As will be discussed in sections 2.1.2 and 2.1.3, high-speed Schottky diodes [16] were used to rectify the signal on the receive side of the plate.

(vi) A*dhesive bondline*. The *bondlines* indicated in Figure 1 were estimated to be 100 μm thick, which was the value used in the modelling discussed in section 2.2. The bondlines were silver loaded epoxy [17] with properties given by Rajic [18] (see the Appendix).

(vi) *Material damping*. The modelling discussed in section 2.2 includes viscous damping in the PZT elements, aluminium plate, and adhesive bondlines.

2.1 Exploration of AEF Power Transfer and Communications

Measurements were made to characterise the reduced-footprint AEF arrangement in terms of its: (i) power transfer efficiency, (ii) battery charging capability, and (iii) upstream communication data rate. Power transfer measurements were performed to allow comparison of the reduced-footprint AEF arrangement with the power transfer capability of larger AEF arrangements previously explored by DSTO. The battery charging and upstream communications experiments were performed as a proof-of-concept that a small-footprint AEF arrangement could be used to provide useful power and data transfer through a metal plate.

2.1.1 AEF Power Transfer with a Linear Load Receiver

Figure 2 is a schematic of the experiment used to investigate the power transfer efficiency of the small-footprint AEF arrangement (termed the *10 mm AEF arrangement*), which for clarity is divided into three sub-components: (i) the *transmitter*, (ii) the *physical interface* and (iii) the *receiver*. The *physical interface* consisted of the arrangement as shown in Figure 1, with the PZT elements mounted using the technique described in reference [7]. Frequency sweeps were carried out across the range 200 to 1500 kHz in 1 kHz steps, and the apparent input power was kept at a constant level of 1 W via computer control of the power amplifier. Constant voltage sweeps across the same frequency range were also performed. The load resistor value was experimentally optimised near the anti-resonant frequency, and found to be 600 Ω for the

10 mm AEF arrangement. Previous work [9] has shown that the optimum load for an AEF formed using Pz26 disk elements with diameter 38 mm and thickness 2 mm was 75 Ω (termed the *38 mm AEF arrangement*). An oscilloscope was used to measure the relevant voltages, with care taken to minimise common-mode errors.

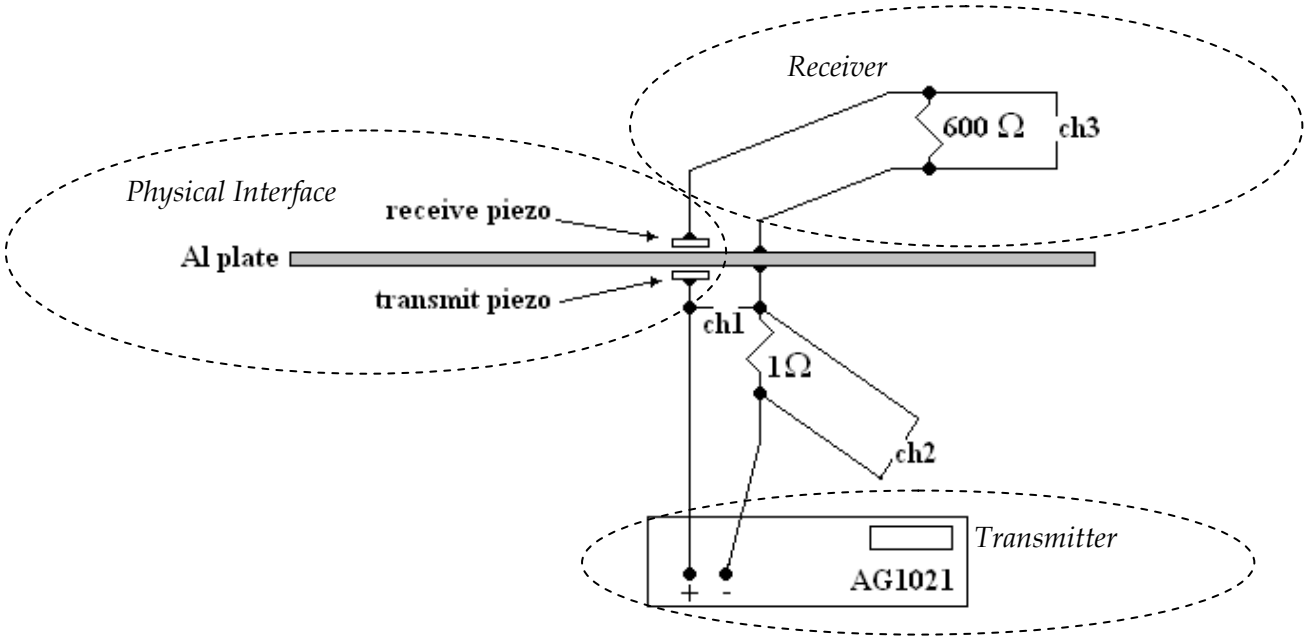

Figure 2: Schematic of the AEF power transfer experiment (600 Ω being the optimum load for the 10 mm AEF arrangement)

2.1.2 AEF Power Transfer for Battery Charging

The previous section described a power transfer experiment where the *receiver's* electrical load was an optimised resistor. Using a resistive load provided insight into the power transfer efficiency of the arrangement. However unless the intention is to use the AEF approach to drive a heating element, for example, a linear resistive load is not a particularly useful load case. One potential application for an AEF system is to charge a battery at a difficult to access location on an aircraft. With this application in mind, an AEF arrangement was connected to the simple battery charge circuitry shown in Figure 3. The battery charge circuit utilised a half-wave rectifier (diodes D1 and D2, BAS70-4 [16]), which was considered more suitable than full-wave rectification since one side of diode D1 may be grounded. A TL431 shunt regulator [19] was used to protect the Li-ion battery from over charging. The output of the shunt regulator was set to 4 V using two resistors (i.e. 1.4 kΩ and 2.4 kΩ), and a 4.7 µF capacitor was used to improve output stability. A 1 Ω test resistor was used to monitor the battery charge current.

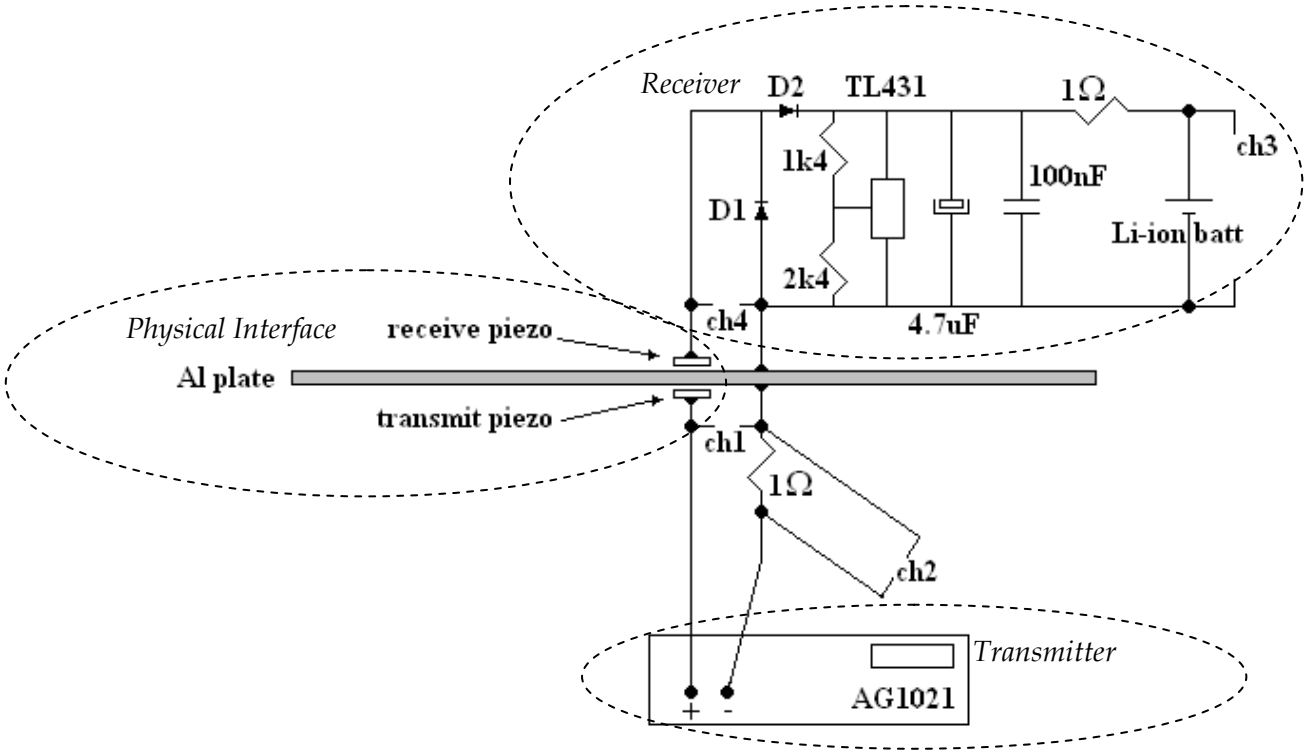

Figure 3: Schematic of the AEF battery charge experiment

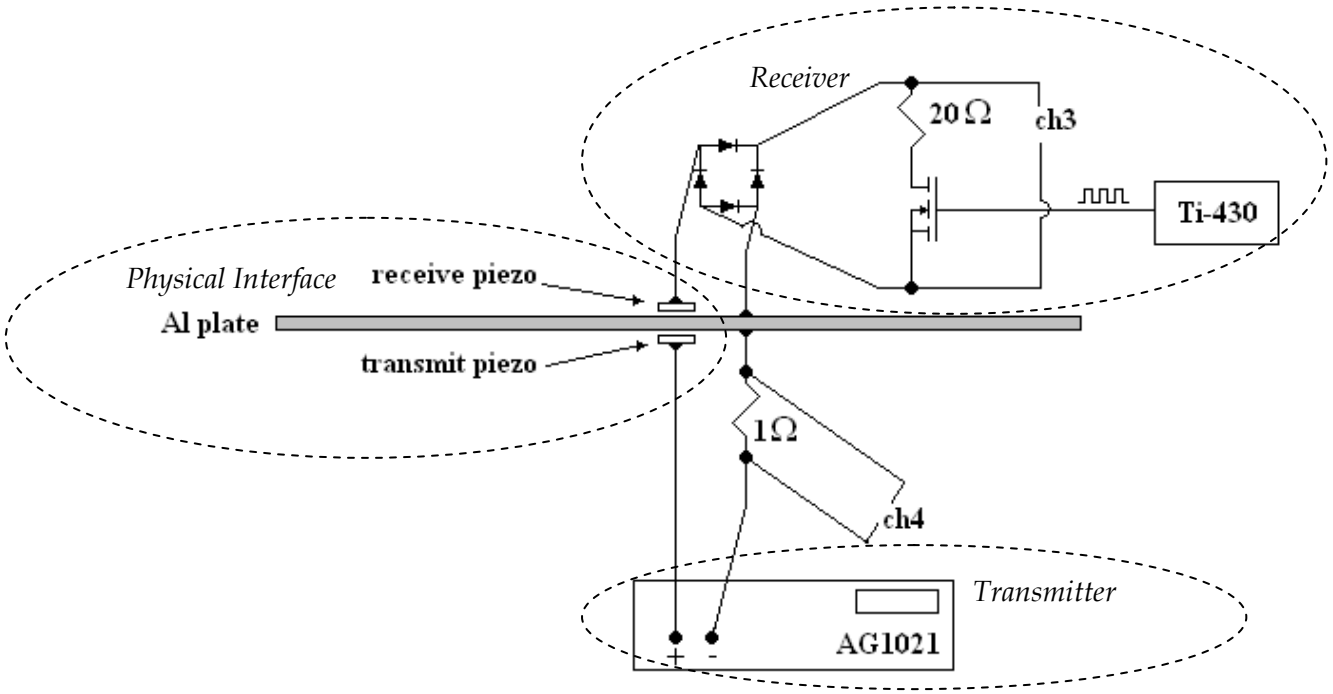

Figure 4: Schematic of the upstream AEF communications experiment

2.1.3 AEF Communications via Receiver Impedance Modulation

It is envisaged that downstream AEF communications (i.e. referring to Figure 4, this involves passing data from the power *transmitter* to *receiver*) will be carried out using on-off keying, and will consist of small amounts of data in the form of short command-packets and check-sum data. Because of the small amount of data involved, the downstream AEF communications is considered non-problematic. Figure 4 shows the schematic of the experiment used to investigate upstream communications (i.e. passing data from the *receiver* to the *transmitter*) which utilised a full-wave rectifier (1N5818 diodes [16]). Upstream AEF communications is considered more technically challenging mainly because of the limited power available at the *receiver* side. One of the upstream communication techniques described in the literature [20] involves modulating the impedance on the *receiver* side, and measuring a corresponding change in voltage on the *transmitter* side. This report will explore the feasibility of using an impedance modulation technique for upstream AEF data communications.

2.2 AEF Modelling

The one-dimensional LTspice AEF model previously developed by the DSTO [7] was based on the assumption of a PZT element geometry approximating a plate, that is with an aspect ratio (defined as *diameter/thickness*) > *10*. The PZT elements used in the *10 mm AEF arrangement* did not satisfy this aspect ratio assumption, so the predictions produced by the one-dimensional model were inaccurate. In physical terms, for most PZT materials the behaviour of a plate-like element is different to that of a cylindrical element due to the action of Poisson's effect. The variation in electro-mechanical behaviour between plate-like and cylindrical elements can clearly be seen in the difference between their respective piezoelectric coupling factors k where,

$$k^2 = \frac{mechanical\ energy\ stored}{electrical\ energy\ applied} \equiv \frac{electrical\ energy\ stored}{mechanical\ energy\ applied}$$

The coupling factor (in the 3-direction) for a plate-like PZT element is designated k_T, and signifies the coupling of electrical and mechanical energy for an element polarised in the thickness direction and vibrating in thickness expansion and compression. The coupling factor (in the 3-direction) for a cylindrical PZT element is designated k_{33}, and has the same polarisation and vibration directions as k_T. The large lateral dimensions of a plate-like PZT element relative to it's thickness imposes a constraint in the form of "lateral clamping" due to Poisson's effect, which leads to k_T being smaller than k_{33} [21, 22]. It should be noted that the lateral clamping on a plate-like PZT element is such that Ristic [23] defines k_T as "*the piezoelectric coupling constant for transversely clamped material* (no motion in the direction transverse to the electric field)." The presence of lateral clamping is the reason why a pure one-dimensional model is sufficient to model a plate-like PZT element, but cannot properly model a cylindrical PZT element with reduced (or zero) lateral clamping.

It was expected that a two-dimensional modelling tool would be required to explore the new small-footprint AEF arrangements examined in this report, which utilise PZT elements with an aspect ratio of five. Two FEM software packages were used. The first package was the ATILA-Light FEM demonstration software [13] (hereafter called 'ATILA') and was chosen

because of its established use on these types of problems [24]. ATILA incorporates the piezoelectric constitutive equations within its FEM formulation, and is specifically designed for modelling piezoelectric systems. The second FEM software package was COMSOL [14] which is a 'multi-physics' platform capable of solving a wide range of scientific problems including those related to piezoelectricity.

An axi-symmetric geometry is shown meshed using quadrilateral elements in Figure 5. The axis of symmetry is shown as a thick line on the left hand edge. The mesh was used to model a single free PZT element, in both the ATILA and COMSOL.

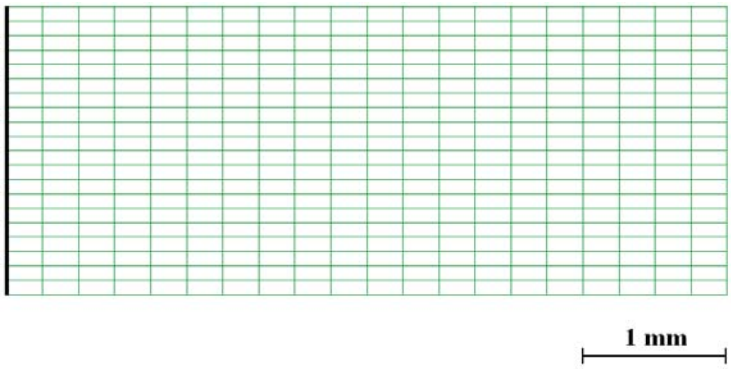

Figure 5: Axi-symmetric FEM model of a single free PZT element with a 20 × 20 mesh

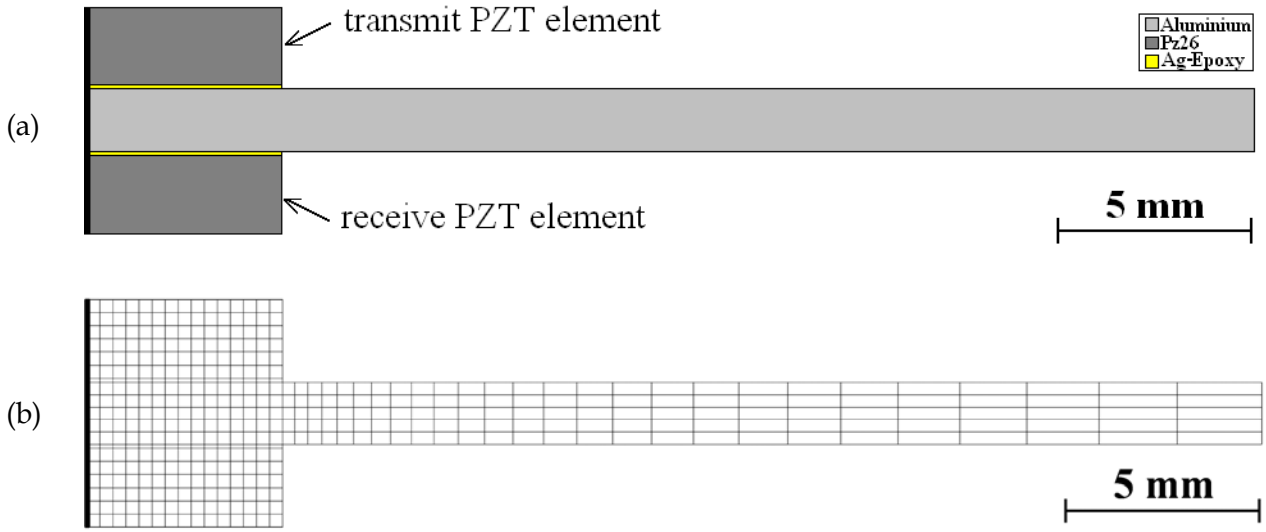

Figure 6: (a) Axi-symmetric FEM model of a PZT/Aluminium/PZT AEF arrangement, including 100 µm Ag-epoxy bondlines, (b) FEM mesh used to model the arrangement

Figure 6a shows the AEF geometry that was investigated using two-dimensional FEM. Again, the axis of symmetry is shown as a thick line on the left hand edge. Figure 6b shows the mesh used to carry out the FEM simulations in COMSOL, with 415 quadrilateral elements. A similar, but not identical, quadrilateral mesh was used to model the AEF geometry in ATILA in order to accommodate the 'degree of freedom' restriction placed on the ATILA-Light software.

3. Results and Discussion

The work is divided into two main parts. The first part will present the measured power transfer, battery charging and communications results from a Pz26 *10 mm AEF arrangement.* Where applicable the measured results will be compared with results obtained previously from Pz26 38 mm AEF arrangements. The second part discusses AEF modelling and compares calculated results with experimental findings. In particular, the failure of one-dimensional modelling will be demonstrated for an AEF arrangement using PZT elements with an aspect ratio of five. Additionally, two-dimensional FEM model predictions of impedance curves, coupling coefficients, mode shapes, and AEF voltage transfer functions will be presented.

3.1 Measured AEF Power Transfer and Communications

The main objective of this report is to show that an AEF arrangement with a small footprint has power transfer and data communication capabilities comparable to that of larger footprint AEF systems [7-9]. To illustrate the magnitude of the AEF footprint reduction, Figure 7 compares the relative footprint size of the *10mm AEF arrangement* described in this report with the *38 mm AEF arrangements* previously examined by DSTO, equating to a ~93% reduction in footprint area.

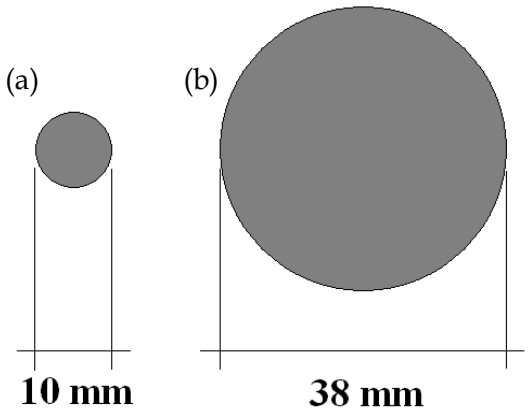

Figure 7: (a) Left hand side is representative of the AEF footprint (with diameter 10 mm) explored in this report, whilst the right hand side (b) illustrates the footprint of previously examined AEF arrangements (with diameter 38 mm)

3.1.1 AEF Power Transfer with a Linear Load Receiver

A schematic of the experimental arrangement used to measure power transfer is given in Figure 2. Shown in Figure 8 is a graph comparing the measured power transfer results from two AEF arrangements. Power transfer sweeps were carried out over the frequency range 200 – 1500 kHz, with the main region of interest being near the fundamental thickness mode anti-resonance frequency, f_{AR} [7-9]. For both AEF arrangements f_{AR} lies somewhere in the range 1000 to 1250 kHz, that is the frequency region that the load resistors were optimised for (600 Ω and 75 Ω respectively). Figure 8 shows that both AEF arrangements, near frequency f_{AR}, have reasonable power transfer efficiencies of 40-50%. Specifically the *10 mm AEF arrangement* had a power transfer maxima of 0.42 W at 1180 kHz, and the *38 mm AEF arrangement* 0.48 W at

1132 kHz. Although the peak power transfer efficiencies are not significantly different, the spectral distributions are. The main spectral effect of reducing the AEF footprint diameter from 38 mm to 10 mm was the appearance of a region of near zero power transfer centred at 1122 kHz. As clearly shown in Figure 8, the Full-Width-Half-Maximum (FWHM) of the set of power transfer peaks near f_{AR} was broader for the *38 mm AEF arrangement* than the *10 mm AEF arrangement*. Discussion regarding the limits of AEF footprint reduction can be found at the end of section 3.2.

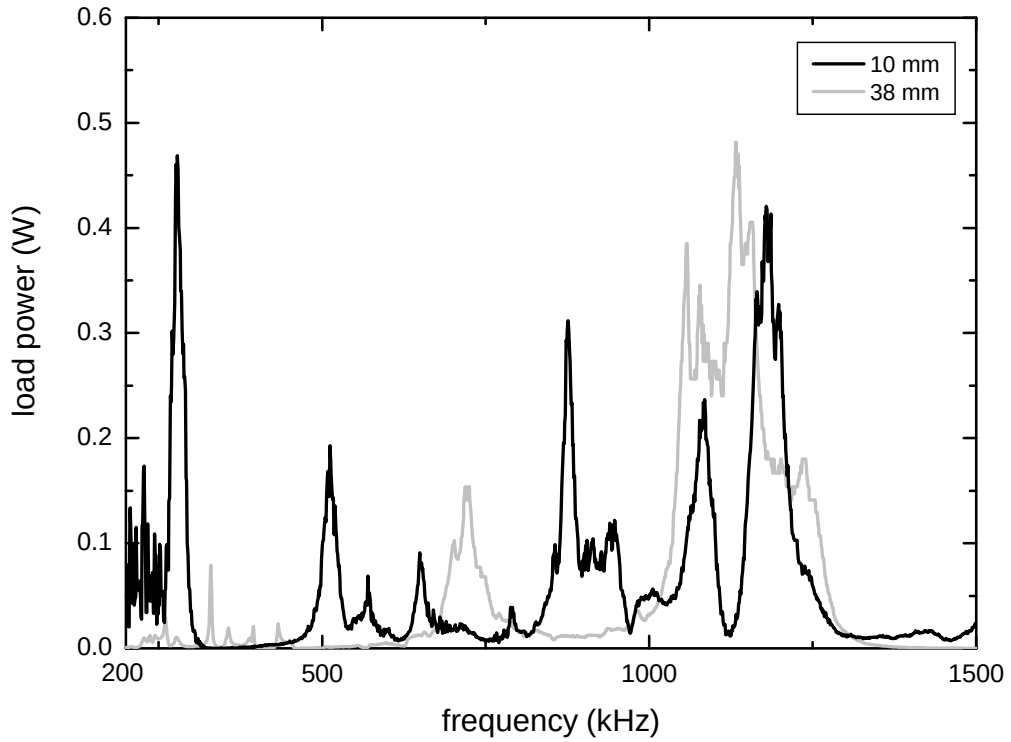

Figure 8: Measured power transfer for two Pz26 based AEF arrangements driven by 1 W of apparent input power. Disk elements were 2 mm thick and either: 10 mm diameter with a 600 Ω resistive load, or, 38 mm diameter with a 75 Ω resistive load.

Figure 8 also shows that the *10 mm AEF arrangement* has reasonable power transfer efficiency at 280 kHz corresponding to the first lateral mode of the 10 mm Pz26 disk elements (note that the load resistor was not optimised at that frequency). Due to equipment limitations it was not possible to perform measurements below 200 kHz. This meant that it was not possible to investigate the power transfer efficiency of the first lateral mode for the *38 mm AEF arrangement*, believed to be located near 58 kHz. Nevertheless, the first lateral mode was not considered for power transfer purposes because the frequency was too low (e.g. 280 kHz) to act as a carrier for the upstream data communications, which required a data transfer rate of 115 kBits per second. Note also that future work will focus on the development of a detachable AEF system. The use of a lateral mode for power transfer is considered incompatible with a detachable AEF system.

3.1.2 AEF Power Transfer for Battery Charging

After determining that reasonable power transfer efficiency was achievable with the *10 mm AEF arrangement*, a battery charge test was performed according to the schematic outlined in Figure 3. It should be noted that one of the design goals of the battery charge circuit was to keep the component count low, since in practice there may be limited board space on the receive side of the AEF arrangement. The AEF drive frequency during the experiment was 1168 kHz. The battery used was an 80 mA.hr Li-ion polymer battery [25] that had been discharged to near 3.2 V. A TL431 [26] shunt regulator circuit was programmed to clamp the battery voltage at 3.96 V, to protect the battery from over-voltage excursions and hence preserve the optimum battery life.

Figure 9a and 9b show respectively the battery voltage and charge current over a 6 hour recharge period. The input power level (as supplied by the power amplifier indicated in Figure 3) was initially chosen so as to produce a 40 mA battery charge current which was expected to result in a standard 4 hour charge cycle. Once set, the amplifier power was not altered during the experiment. At the end of the recharge cycle it was expected that the battery voltage would be near 4 V. However during the course of the experiment the measured input power slowly oscillated (apparent in Figure 9a and 9b) with an average of 1.78 W. Due to the slow oscillations in the input power the Li-ion battery only managed to charge to ~3.8 V over a 6 hour period. The oscillation in input power was later found to be related to laboratory temperature variations produced by air-conditioner cycling (cycling which varies on a day-to-day basis according to the outside temperature). A number of weeks after the battery charge experiment the laboratory temperature was measured over an extended period, the results of which are shown in Figure 9c. It is believed that the laboratory temperature variations affected the output power of the power amplifier. Further work is being undertaken to determine the relationship between AEF power transfer efficiency and temperature.

3.1.3 AEF Communications via Receiver Impedance Modulation

Previous work at DSTO has indicated that an upstream AEF data communication rate of 115 kBits per second was feasible. Specifically, in reference [9] data communication using a pulsed method for bit transfer was demonstrated for a *38 mm AEF arrangement*. The literature [20] outlines an impedance modulation technique for upstream data communications. It was decided that the impedance modulation approach would be tested in conjunction with the *10 mm AEF arrangement* examined in this report, with the aim of confirming that data rates of 115 kBits per second were feasible.

(a)

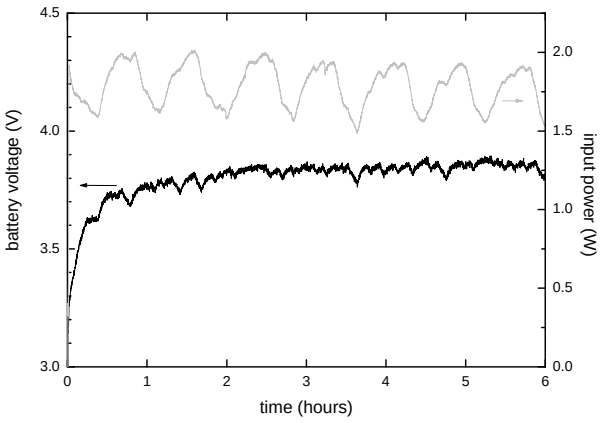

(b)

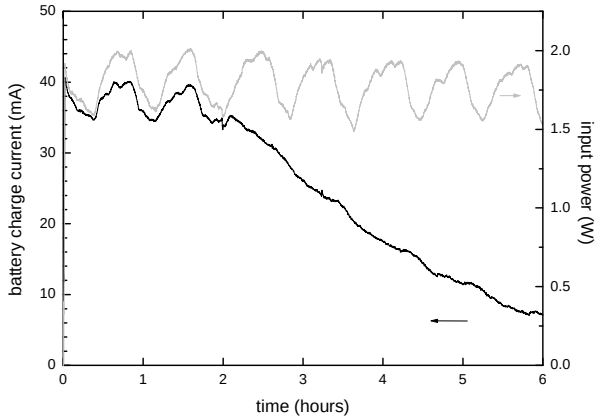

(c)

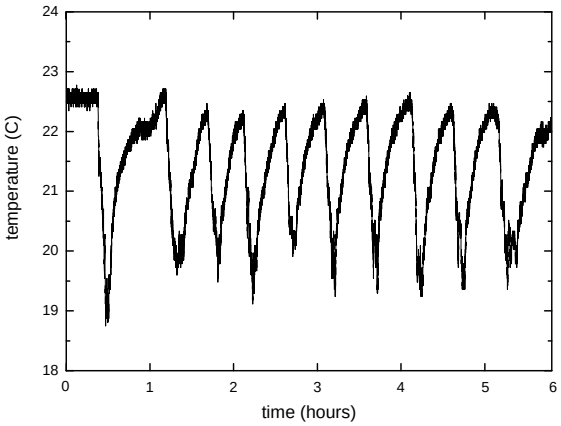

Figure 9: Measured curves showing: (a) battery charge voltage, (b) battery charge current and (c) laboratory temperature.

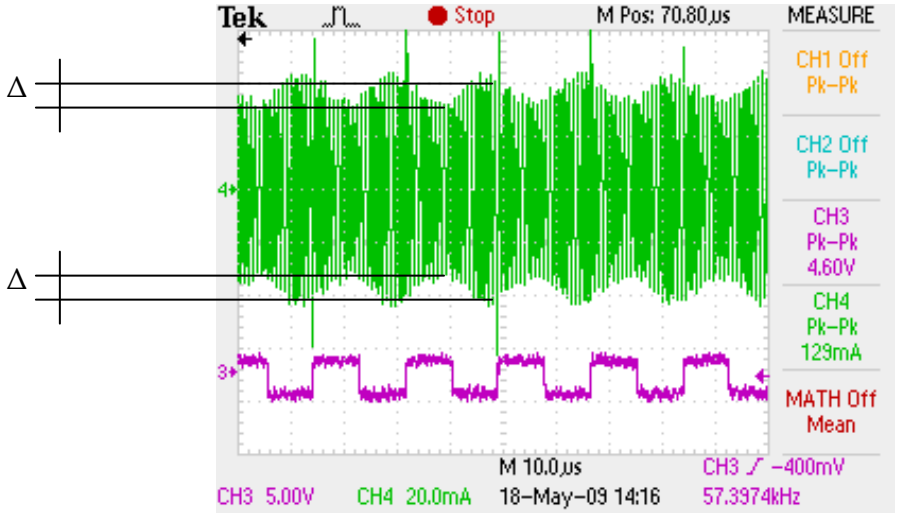

Figure 10: Measured upstream AEF data communications. Channel locations are shown in Figure 4, with CH3 being the modulated load voltage, and CH4 the resultant input current measured using a 1 Ω sense resistor. Modulation depth of the peak-to-peak input current was 2Δ ~ 20 %.

Figure 4 shows a schematic of the experiment that was performed to test AEF upstream data communications with impedance modulation. Preliminary communication results are given in Figure 10, which shows the voltage across the electrical load (CH3) as it is modulated between a 20 Ω short and open circuit, and the resultant modulated input current waveform (CH4). As shown in Figure 10, the ~115 kBits per second load impedance modulation (with the binary pattern alternating between one and zero) induced a modulation depth of 2Δ ~ 20% in the amplitude of the peak-to-peak input current (CH4). The authors consider that it is technically feasible to extract data from this level of modulation in the input current waveform, and hence conclude that it is possible to perform upstream data communications using the impedance modulation approach with a reduced footprint AEF arrangement.

3.2 AEF Modelling

In section 2.2 it was explained that predictions from the previously developed one-dimensional AEF model [7-9] were unreliable for the *10 mm AEF arrangement* examined in this report, due to the aspect ratio of the 2 mm thick Pz26 elements. To demonstrate this unreliability, Figure 11 compares the measured and predicted load voltage for a *10 mm AEF arrangement* driven by a constant 20 V_{RMS} input voltage and with a 600 Ω resistive load. Measured results were collected using the experimental setup depicted in Figure 2.

One-dimensional model results were generated with an LTspice AC-analysis using methods described previously [7-9]. Figure 11 shows that the predictions of the one-dimensional model are incorrect across most of the frequency range, with the exception being the peak near 1168 kHz, thought to be related to the thickness mode anti-resonant frequency. The one-dimensional model may have predicted an accurate response at the anti-resonant frequency due to the PZT thickness-displacement amplitude being at a local minimum. More work would be required to confirm this, and nonetheless, the one-dimensional model would still be

of little use due to the multi-frequency nature of an AEF arrangement that is simultaneously transferring power and data.

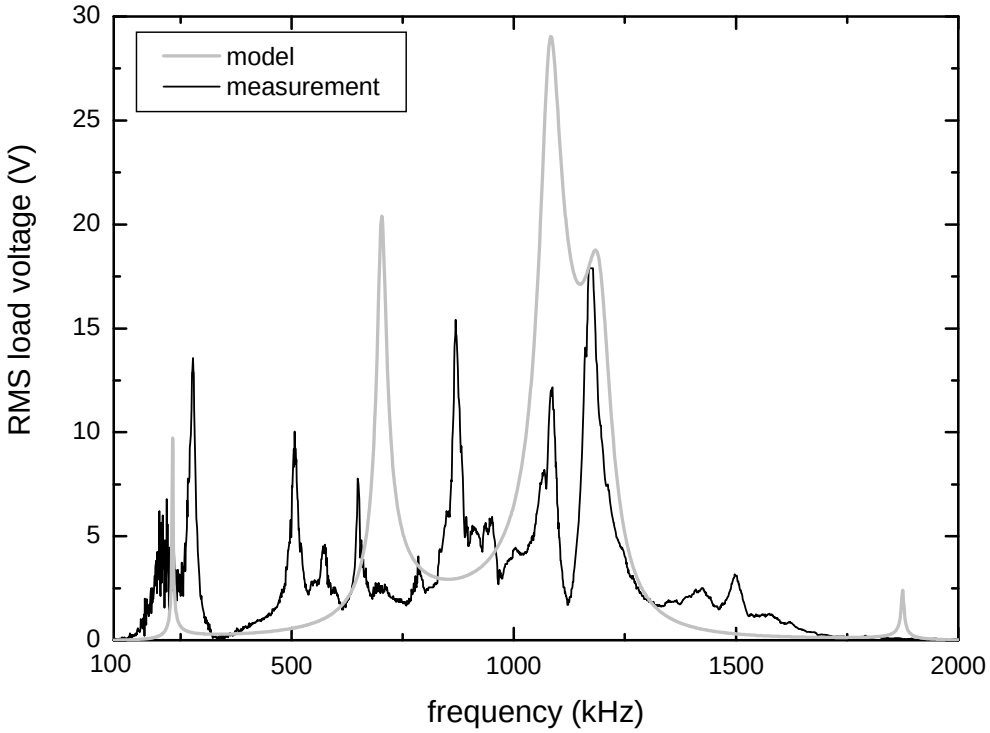

Figure 11: Comparison of model predictions with measured results for a 10 mm AEF arrangement, using a 20 V_{RMS} input voltage and with a 600 Ω resistive load.

Due to the failure of the one-dimensional modelling, it was believed that a more detailed two-dimensional model would be required to generate accurate predictions of steady-state AEF power transfer, and other behaviours such as the transient effects produced during data communications. Prior to modelling a full AEF arrangement, the initial FEM work was focused on modelling the impedance curves of single free Pz26 elements. The Pz26 piezoelectric parameters that were used for FEM modelling were found at the manufacturer's website, and are duplicated in the Appendix. Note that two separate sets of Pz26 piezoelectric parameters are provided by the manufacturer, a 'standard' set and an 'FEM' set. The piezoelectric parameters are used to form the elasticity, piezoelectric coupling and relative permittivity matrices required for FEM modelling.

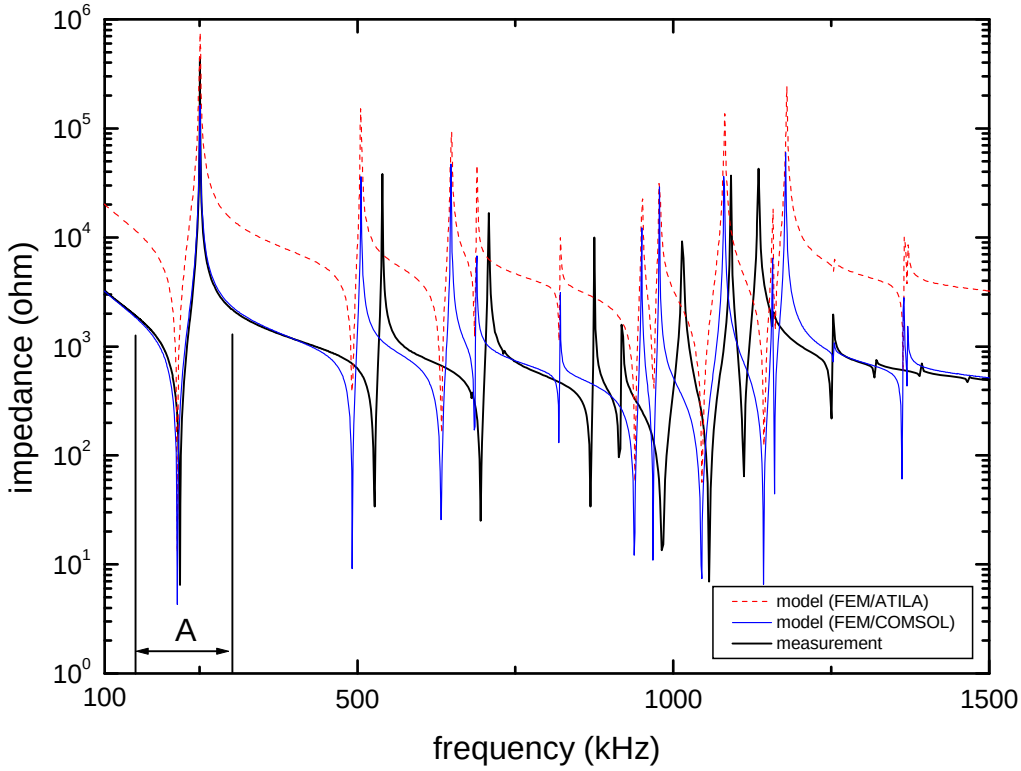

Figure 12: Model predictions and measured results for a single Pz26 disk element with diameter 10 mm and thickness 2 mm. FEM modelling was performed using the 'standard' piezoelectric parameters and a 20 × 20 mesh.

The validity of the FEM results was tested by comparing measured impedance curves from a free Pz26 disk element with diameter 10 mm and thickness of 2 mm, with model predictions using the FEM geometry shown in Figure 5.

Figure 12 compares measured and predicted (FEM model) impedance curves for a single free Pz26 disk element, with FEM modelling performed using 'standard' piezoelectric parameters (see the Appendix) and the mesh shown in Figure 5. Good correlation can be seen between the measured and FEM modelled resonant peak between 150-280 kHz (labelled region 'A' in Figure 12), corresponding to the first lateral mode of the 10 mm diameter disk. It seems to be a reasonable assumption that the 'standard' piezoelectric parameters were determined from an optimisation process focusing on the first lateral mode. Other than at the first lateral mode, Figure 15 shows poor correlation between the measured and modelled impedance curves. In terms of impedance magnitude, the COMSOL prediction is well matched to the measured curve however there is an unexplained impedance offset seen in the impedance data predicted by the ATILA package.

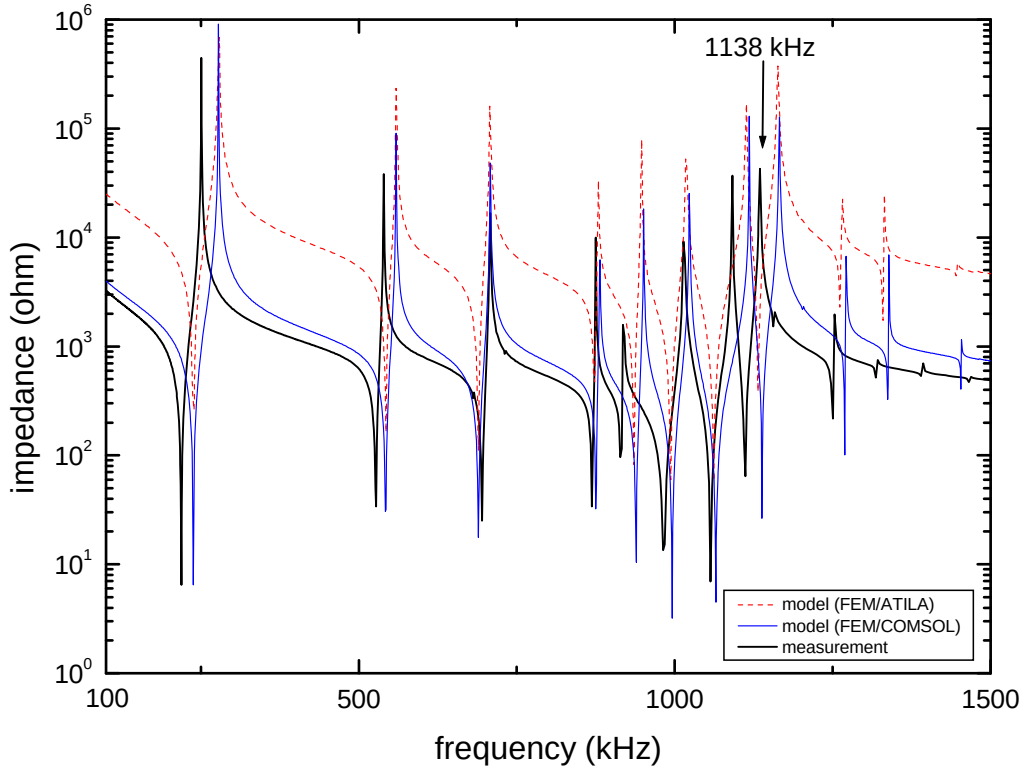

Figure 13: Model predictions and measured results for a single Pz26 disk element with diameter 10 mm and thickness 2 mm. FEM modelling was performed using the 'FEM' piezoelectric parameters and a 20 × 20 mesh.

The 'FEM' piezoelectric parameters (see the Appendix) were used to generate the FEM modelled impedance curves shown in Figure 13. The model predictions shown in Figure 13 compare reasonably well with the measured results across the entire frequency range, although the correlation with the first lateral mode (150-280 kHz) has somewhat degraded compared with that shown in Figure 12. Again, there is an unexplained offset in the ATILA impedance magnitudes. Of note is the relatively large number of resonant peaks in the vicinity of the frequency f_{AR} (i.e. ~1138 kHz) due to the aspect ratio of the disk and the large mechanical Q of the Pz26 material. Note that the modelling of the impedance curves ignored the effects caused by temperature and mechanical clamping (see reference [7] for the method used to measure the impedance curves of a free PZT element). Based on the better overall agreement shown in Figure 13 it was decided that FEM modelling of the *10 mm AEF arrangement* would be performed using the 'FEM' set of piezoelectric parameters given in the Appendix.

The *10 mm AEF arrangement* shown in Figure 6a was modelled with FEM, and where applicable the simulation results were compared with measured data. Specifically, FEM modelling the AEF arrangement was used to: (i) carry out a 'modal resantires' analysis to model the piezoelectric coupling coefficients of the first 150 vibration modes, (ii) produce visualisations of the various resonant mode shapes, and (iii) produce voltage transfer versus frequency curves.

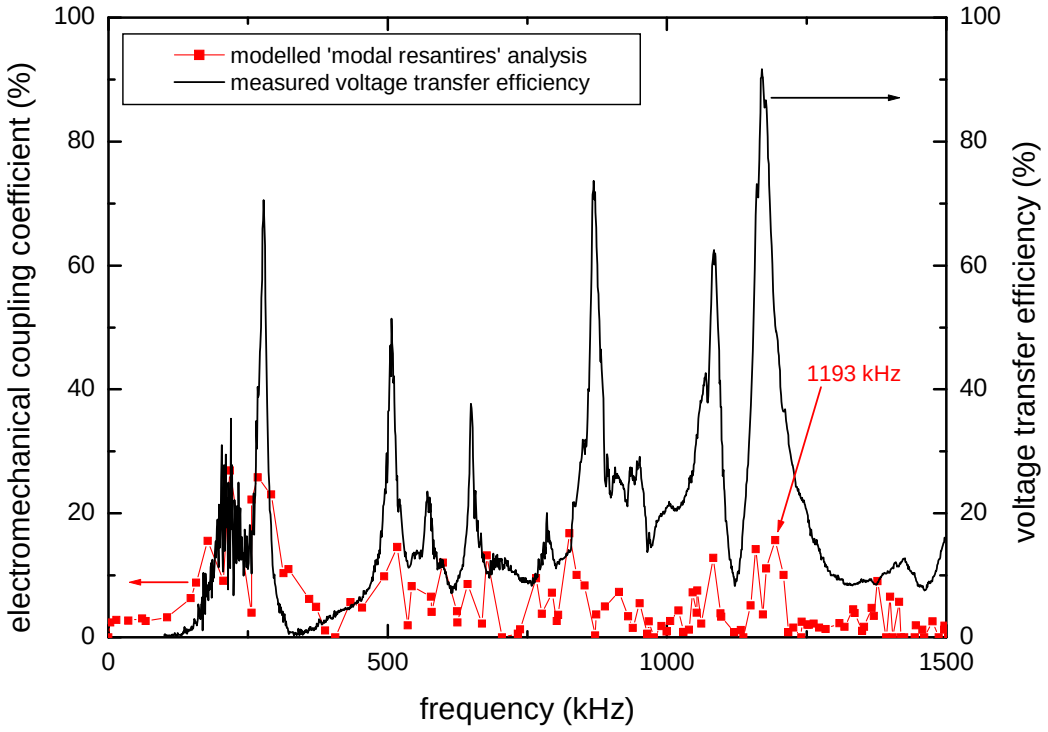

Figure 14: Piezoelectric coupling coefficients (predicted by ATILA) and measured voltage transfer efficiency for a 10 mm AEF arrangement.

Using ATILA, a 'modal resantires' analysis was performed on the *10 mm AEF arrangement* shown in Figure 6a, which is an analysis that finds the first *N* vibration modes of a structure taking into account the piezoelectric properties of any piezo-active materials present in the structure [13]. For each vibration mode that is found, ATILA outputs a resonant frequency and a calculated electromechanical coupling coefficient (which is an electrical-to-mechanical conversion efficiency). Figure 14 compares an FEM 'modal resantires' analysis (*N=150*) with a measured voltage transfer sweep, where the sweep was performed using the experimental arrangement shown in Figure 2 with an input voltage 20 V_{RMS} and with a 600 Ω resistive load. As indicated by the 'modal resantires' result, the *10 mm AEF arrangement* has a relatively large number of resonant peaks across the entire frequency (100-1500 kHz), which can be related to the resonant modes of a free Pz26 element (e.g. shown in Figure 13). Figure 14 shows that each peak in the measured voltage transfer curve appears to correspond to one or more calculated 'modal resantires' vibration modes. Note that the lines joining the 'modal resantires' point-results (in Figure 14) are only provided to guide the eye.

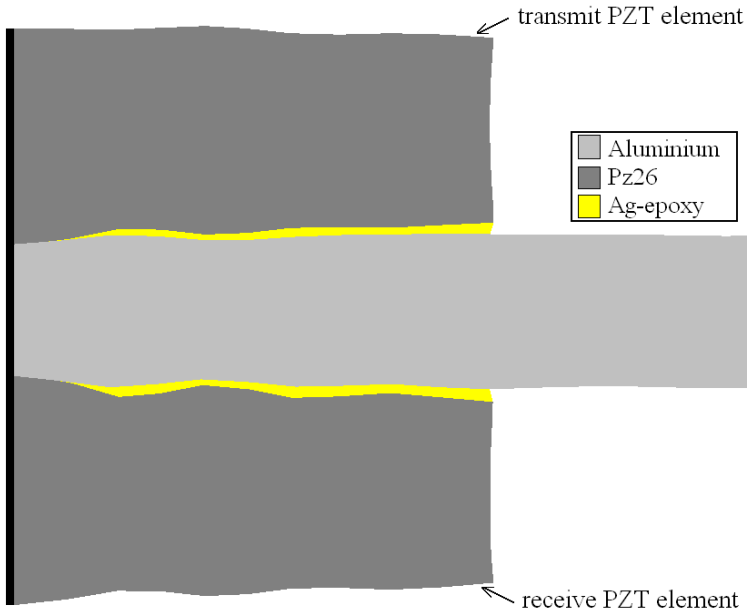

Figure 15: ATILA simulation of the thickness resonant mode at 1193 kHz

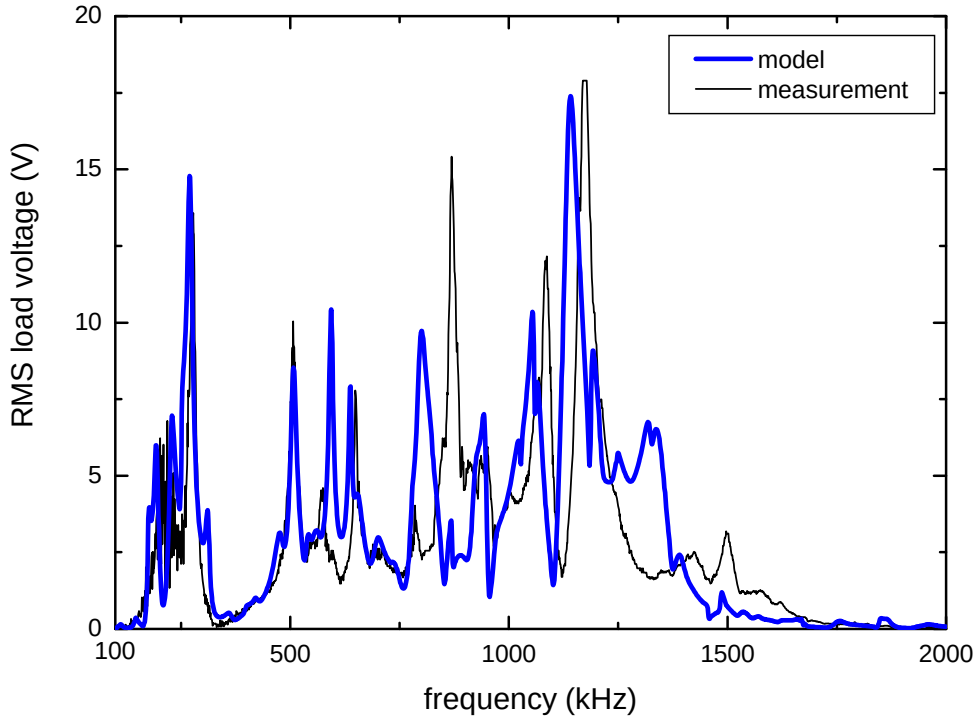

Figure 16: Measured and predicted (by COMSOL) voltage transfer results for a 10 mm AEF arrangement, using a 20 V_{RMS} input voltage and with a 600 Ω resistive load

Given that the *10 mm AEF arrangement* has a large number of resonant modes across the frequency range 200-1500 kHz (i.e. as shown in Figure 14), it was particularly useful to be able to visualise the physical behaviour of the vibration modes. ATILA has the capability of producing a two-dimensional visualisation from the results of an axi-symmetric two-dimensional model. As a demonstration, there is an arrow in Figure 14 pointing at what

appears to be the main thickness mode resonance at 1193 kHz. Figure 15 shows an ATILA visualisation of the 1193 kHz mode shape for the *10 mm AEF arrangement* (Figure 6a shows the original geometry). Future work will examine the bondline stresses induced by various vibration modes, and may provide an indication of which mode is preferable in terms of both power transfer and robustness of the AEF system.

COMSOL has the capability of combining multi-physics modelling with models of discrete electronic components (e.g. as used in LTspice [12]). Using this capability, a COMSOL model of the experiment depicted in Figure 2 was created and then used to predict the voltage transfer spectrum of a *10 mm AEF arrangement*. The model included an input voltage of 20 V_{RMS} and a 600 Ω resistive load. Figure 16 shows results from the model compared with measured results from a near identical physical experiment. The measured results were shown previously in Figure 11. As mentioned in section 2, the physical experiment was performed using a 600 mm square aluminium plate that was clamped in each corner and resting on a wooden bench, whereas the axi-symmetric COMSOL model was effectively circular with a 300 mm diameter and 'floating' in space. To allow a useful comparison with experiment it was necessary to model the aluminium plate with a mechanical *Q* of *20*, which is significantly smaller than the actual mechanical *Q* of the plate. It is thought that the model required extra damping to approximate the acoustic losses produced by the clamping of the plate in the physical experiment. All other material parameters used in the modelling are given in the Appendix, with the 'FEM' Pz26 parameters used to model the disk elements. Figure 16 shows good correlation between the modelled and measured voltage transfer curves, indicating that COMSOL FEM modelling has sufficient fidelity to assist in the optimisation of future AEF designs.

There are a number of considerations that may limit the footprint reduction of an AEF arrangement. For a given power transfer requirement, and assuming that the thickness of the PZT elements used in an AEF arrangement is constant (e.g. 2 mm as used in this report) then as the footprint (i.e. diameter) of the PZT elements decreases:

- The impedance value of the optimised *receiver* load increases, resulting in increased load voltages. Eventually a limit would be reached when the AEF voltages become large relative to the de-poling voltage of the PZT elements, leading to non-linear behaviour and reducing the life of the AEF arrangement.
- There may be an excessive temperature increase due to viscous damping in the AEF materials and bondlines, resulting in thermal de-poling of the PZT elements and so reducing the life of the AEF arrangement.
- The maximum electrical power density of the piezoelectric material would be reached.
- The spectral effect on the FWHM of the first thickness mode is unknown. If the FWHM became too narrow it would become technically difficult to utilise the first thickness mode for AEF power transfer. For these reasons, the authors believe that (for a specific power transfer requirement) there is a limit to how far an AEF footprint can be reduced. A full investigation of the limit of the AEF footprint reduction is beyond the scope of this report, however it is expected that an AEF with a diameter of less than 10 mm will be capable of transmitting 1 W of power with a data transfer rate of 115 kBits per second. An AEF formed using piezoelectric elements of 6.35 mm diameter and 0.5 mm thickness is currently being investigated.

4. Conclusion

This report has examined the modelling, characterisation and manufacture of an Acoustic Electric Feedthrough (AEF) arrangement with a significant footprint reduction compared with AEF geometries previously examined by DSTO. The ultimate aim of the work is to develop a small, robust, detachable AEF system capable of passing power and communications through the aluminium skin of an aircraft using ultrasound. An AEF arrangement operates via two piezoelectric elements, located collinearly on opposite sides of a metal plate. A piezoelectric element is excited at its thickness mode anti-resonance frequency producing ultrasound that passes through the metal plate to be received by a second element located on the opposite side of the plate. Earlier AEF arrangements investigated by DSTO had a 38 mm diameter. The AEF arrangement examined in this report had a diameter of 10 mm, equating to footprint reduction of 93%. This report has demonstrated that a *10 mm AEF arrangement:* (i) has a power transfer efficiency of 42%, (ii) with a 1 W input can transfer 420 mW of real power, and (iii) can transfer data at a rate of 115 kBits per second. These power and data transfer capabilities are equivalent to those previously reported for a *38 mm AEF arrangement*. This report also demonstrated that a *10 mm AEF arrangement* is capable of charging an 80 mA.hr Li-ion battery. Lastly, it was discovered that the one-dimensional AEF models previously developed by the DSTO were not sufficiently accurate to model the *10 mm AEF arrangement* investigated in this report, due to the aspect ratio of the PZT elements employed. Two-dimensional FEM models were developed and were shown to have sufficient fidelity to assist with future AEF design and optimisation.

5. References

1. S. Galea, S. van der Velden, S. Moss, I. Powlesland, "On the Way to Autonomy: the Wireless-interrogated and Self-powered 'Smart Patch' System," Encyclopedia of Structural Health Monitoring, Editors-in-Chief: C. Boller, F. K. Chang and Y. Fujino, Chpt. 76, John Wiley & Sons, ISBN 978-0-470-05822-0, 2009

2. S. Galea, T. Trueman, L. Davidson, P. Trathen, B. Hinton, A. Wilson, T. Muster, I. Cole, P. Corrigan and D. Price, "Aircraft structural diagnostic and prognostic health monitoring for corrosion prevention and control," Encyclodepia of Structural Health Monitoring, Editors-in-Chief: C. Boller, F. K. Chang and Y. Fujino, Chpt. 112, John Wiley & Sons, ISBN 978-0-470-05822-0, 2009

3. S. D. Moss, S. C. Galea, I. G. Powlesland, M. Konak, A. A. Baker., "In-situ health monitoring of a bonded composite patch using the strain ratio technique," *Proceedings of SPIE*, Vol. 4325, Paper 4235-41, 2000

4. C. Davis, W. Baker, S. Moss, S. Galea, R. Jones, "In situ health monitoring of bonded composite repairs using a novel fibre Bragg grating sensing arrangement," *Proceedings of SPIE*, Vol. 4934, pp. 140-149, 2002

5. N. Rajic, "Development of an Active Smart Patch for Aircraft Repair," Encyclopedia of Structural Health Monitoring, Editors-in-Chief: C. Boller, F. K. Chang and Y. Fujino, Chpt. 107, John Wiley & Sons, ISBN 978-0-470-05822-0, 2009

6. S. Galea and I. Powlesland, "Caribou Loads Flight Survey Using A Rapid Operational Loads Measurement Approach", *Materials Forum*, Vol. 33, pp. 100-109, 2009

7. S. Moss, P. McMahon, M. Konak, C. Phoumsavanh, N. Rajic, S. Galea, I. Powlesland, "Modelling and Experimental Validation of an Acoustic Electric Feedthrough," DSTO-RR-0338

8. S. Moss, M. Konak, C. Phoumsavanh, K. Tsoi, I. Powlesland, "Acoustic Electric Feedthrough Demonstrator Mk-I," DSTO-TR-2296

9. S. Moss, C. Phoumsavanh, M. Konak, K. Tsoi, N. Rajic, S. Galea, I. Powlesland, P. McMahon, "Design of the Acoustic Electric Feedthrough Demonstrator Mk-II," *Materials Forum,* Vol. 33, pp. 187-200, 2009

10. Y. Hu, X. Zhang, J. Yang, Q. Jiang, "Transmitting Electric Energy Through a Metal Wall by Acoustic Waves Using Piezoelectric Transducers," *IEEE Trans. Ultrason., Ferroelect., Freq. Cont.,* Vol. 50, No. 7, pp. 773-781, 2003

11. S. Sherrit, M. Badescu, X. Bao, Y. Bar-Cohen, Z. Chang, "Efficient electromechanical Network Models for Wireless Acoustic-Electric Feedthroughs," *Proceedings of SPIE,* Vol. 5758, 2005

12. M. Engelhardt, LTspice IV, Linear Technology Corporation, www.linear.com, last accessed 2009

13. K. Uchino, "FEM and Micromechatronics with ATILA Software," CRC Press, ISBN 978-1-4200-5878-9, 2008

14. COMSOL AB, "COMSOL Multiphysics User's Guide," Version 3.5a, November 2008

15. Piezoelectric material parameters, Ferroperm website, www.ferroperm.com, last accessed April 2009

16. http://www.fairchildsemi.com/pf/1N/1N5818.html, last accessed June 2008, or, http://www.datasheetcatalog.org/datasheet/siemens/BAS70-04.pdf, last accessed July 2009

17. Circuitworks Conductive Epoxy, CW2400

18. N. Rajic, "A model for the piezoelectric transduction of stress waves," *Smart Mater. Struct.,* Vol. 15, pp.1151-1164 , 2006

19. http://focus.ti.com/docs/prod/folders/print/tl431.html, last accessed June 2009

20. D. A. Shoudy, G. J. Saulnier, H. A. Scarton, P. K. Das, S. Roa-Prada, J. D. Ashdown, and A. J. Gavens, "An Ultrasonic Through-Wall Communication System with Power Harvesting," *IEEE Ultrasonics Symposium*, pp. 1848-1853, 2007

21. S. M. Peelamedu, "Piezoelectric Effect and Its Applications", Encyclopedia of Optical Engineering, Vol. 3, pp. 2097-2099, CRC Press, ISBN 978-0-824-74252-2, 2003

22. J. A. Hossack, B. A. Auld, "Advanced Modelling and Optimisation of Piezoelectric Composites," Final Tech. Rep. 6/01/90 - 5/31/92, p.66 and p.106, *Stanford University* for the *Office of the Chief of Naval Research*, AD-A253 800, July 1992

23. V. M. Ristic, "Principles of Acoustic Devices," John Wiley and Sons, New York, p. 138, 1982

24. T. Bove, W. Wolny, E. Ringgard, K. Breboel, "New Type of Piezoelectric Transformer with Very High Power Density," *Proceedings of the 12th IEEE Symposium on Applications of Ferroelectrics*, Vol. 1, pp. 321-324, 2000

25. http://www.gmbattery.com/dl/cp11/li-ion/LIPO/BlueTooth/GMB041225.PDF, last accessed July 2009

26. http://www.datasheetcatalog.com/datasheets_pdf/T/L/4/3/TL431.shtml, last accessed July 2009

Appendix: Parameter Values Used in Calculations

Definition	Designation	Units	Material			
			Pz26 'standard' [15]	**Pz26 'FEM'** [15]	**aluminium** [18]	**silver epoxy** [18]
elastic modulus	Y	GPa	-	-	73.1	7.28
density	ρ	kg/m^3	7700	7650	2770	3890
mechanical quality	Q	-	3023	3023	1000	23.4
relative permittivity	$\varepsilon^T_{11,rel}$	-	1190	1310	-	-
	$\varepsilon^T_{33,rel}$	-	1330	1080	-	-
piezoelectric strain coefficients	d_{31}	C/N	-1.28e-10	-1.06e-10	-	-
	d_{33}	C/N	3.28e-10	2.77e-10	-	-
	d_{15}	C/N	3.27e-10	3.50e-10	-	-
elastic compliances	s^E_{11}	m²/N	1.30e-11	1.22e-11	-	-
	s^E_{12}	m²/N	-4.35e-12	-5.13e-12	-	-
	s^E_{13}	m²/N	-7.05e-12	-5.13e-12	-	-
	s^E_{33}	m²/N	1.96e-11	1.60e-11	-	-
	s^E_{44}	m²/N	3.32e-11	3.67e-11	-	-

DEFENCE SCIENCE AND TECHNOLOGY ORGANISATION
DOCUMENT CONTROL DATA

1. PRIVACY MARKING / CAVEAT (OF DOCUMENT)

2. TITLE

Footprint Reduction for the Acoustic Electric Feedthrough Technique

3. SECURITY CLASSIFICATION (FOR UNCLASSIFIED REPORTS THAT ARE LIMITED RELEASE USE (L) NEXT TO DOCUMENT CLASSIFICATION)

Document	(U)
Title	(U)
Abstract	(U)

4. AUTHOR(S)

Scott Moss, Jeremy Skippen, Michael Konak and Ian Powlesland

5. CORPORATE AUTHOR

DSTO Defence Science and Technology Organisation
506 Lorimer St
Fishermans Bend Victoria 3207 Australia

6a. DSTO NUMBER	6b. AR NUMBER	6c. TYPE OF REPORT	7. DOCUMENT DATE
DSTO-TR-2395	AR-014-730	Technical Report	March 2010

8. FILE NUMBER	9. TASK NUMBER	10. TASK SPONSOR	11. NO. OF PAGES	12. NO. OF REFERENCES
2009 / 1078496	AIR 07 / 053	DGTA	22	26

13. URL on the World Wide Web

http: / / www.dsto.defence.gov.au / corporate / reports / DSTO-TR-2395.pdf

14. RELEASE AUTHORITY

Chief, Air Vehicles Division

15. SECONDARY RELEASE STATEMENT OF THIS DOCUMENT

Approved for public release

OVERSEAS ENQUIRIES OUTSIDE STATED LIMITATIONS SHOULD BE REFERRED THROUGH DOCUMENT EXCHANGE, PO BOX 1500, EDINBURGH, SA 5111

16. DELIBERATE ANNOUNCEMENT

No Limitations

17. CITATION IN OTHER DOCUMENTS Yes

18. DSTO RESEARCH LIBRARY THESAURUS http: / / web-vic.dsto.defence.gov.au / workareas / library / resources / dsto_thesaurus.shtml

smart structures, smart materials, piezoelectric materials, power engineering, communications engineering

19. ABSTRACT

This report outlines progress towards reducing the footprint of the DSTO Acoustic Electric Feedthrough (AEF). The AEF approach is being explored as a potential means of wirelessly powering in situ structural health monitoring systems embedded within aircraft and other high value assets. In previous work it was shown that power and data communications can be transmitted ultrasonically through thin aluminium plate using an AEF formed with 38 mm diameter piezoelectric disks. In this report it is shown that a small-sized AEF system formed using 10 mm diameter piezoelectric disks (equating to a footprint reduction of 93%) has a power transfer efficiency of 42% and data transfer rate of 115 kBits per second, equivalent to the capabilities of the previously examined AEF arrangments with significantly larger footprint. Two-dimensional finite-element models are developed and shown to have sufficient fidelity to assist with future AEF design and optimisation.